RSC Applied Polymers

ROYAL SOCIETY OF CHEMISTRY

PAPER

View Article Online
View Journal



Cite this: DOI: 10.1039/d6lp00048g

# Tailored imprinted polymers for selective recognition of sulfonated dyes: extraction of dyes from soft drinks, water and food samples

Krushna Shinde, † Rupali Thorave *† and Sudhirkumar Shinde *

Synthetic sulfonated food dyes in beverages and processed foods pose health and environmental risks due to their persistence and potential toxicity. Traditional detection methods for these dyes lack selectivity and involve excessive solvent use. Herein, we report the synthesis of molecularly imprinted polymers (MIPs) featuring high affinity and enhanced capacity for binding to sulfonated dyes. The MIPs were prepared using phenyl sulfonic acid (PSA) as a template, a tweezer-type bis-imidazolium functional monomer, 2-hydroxyethyl methacrylate (HEMA) co-monomer, and ethylene glycol dimethacrylate (EGDMA) crosslinker. The recognition performance of the PSA-imprinted MIPs was evaluated *via* rebinding isotherm data, fitted to the mono-Langmuir isotherm model, which revealed binding capacities ranging from 100–300 μmol $g^{-1}$ with $10^3$–$10^4$ $M^{-1}$ affinity in organic and aqueous solvents. The optimized MIPs demonstrated superior affinity for a wide range of structurally diverse sulfonated dyes containing a PSA substructure. Their practical applicability was confirmed through successful recognition of commercial dyes in water, soft drinks, and food matrices, including the successful capture of food dye from adulterated turmeric samples. As a proof-of-concept, class-selective MIPs were employed as adsorbents in solid-phase extraction (SPE) cartridges, effectively capturing trace amounts of sulfonated dyes from water. Collectively, these results underscore the potential of the developed MIPs for food monitoring and environmental remediation.

Received 10th February 2026,
Accepted 3rd May 2026

DOI: 10.1039/d6lp00048g

rsc.li/rscapplpolym



## Introduction

The estimated worldwide annual production of synthetic dyes exceeds $7 \times 10^5$ tons. These dyes are widely utilized across diverse industries, including the dyeing of textiles, paper, pulp, and plastic, as well as being used in coloring agents, photographs, foods, cosmetics, and other industrial applications.[1] According to Grand View Research (GVR, 2023), the global food coloring market size was valued at USD 3.13 billion in 2023, and it is expected to grow at a compound annual growth rate (CAGR) of 6.5% from 2024 to 2030.[2] Synthetic food dyes, particularly sulfonated aromatic compounds and sulfonated azo dyes, are extensively used to enhance the visual appeal of beverages, confectionery, and processed foods.[3] Among these, tartrazine (TZ, E102), Sunset Yellow (SY, E110), carmoisine (E122), amaranth (AM, E123), ponceau 4R (E124), Allura Red AC (E129), Brilliant blue (E 133), and HT Brown (E155) are the most utilized.[4,5]

There are significant ecological consequences when sulfonated azo dyes are released into aquatic environments. These compounds interfere with light penetration by altering sunlight absorption and reflection, thereby disrupting the photosynthetic activity and biological functioning of aquatic organisms. In addition, they can reduce dissolved oxygen levels, ultimately leading to the degradation of aquatic ecosystems. Synthetic azo dyes and degradation products such as aromatic amines are compounds classified as possible human carcinogens and are associated with potential health risks and overall ecological toxicity.[6] The continued application of these colorants raises concern regarding their long-term effects.

Regulatory agencies, including the European Food Safety Authority (EFSA) and the US Food and Drug Administration (FDA), have established guidelines to control their use and ensure consumer safety.[7,8] Nevertheless, despite extensive research on dietary exposure and associated health risks, the data remain controversial. Acceptable intake limits have been proposed; however, certain studies emphasize the need for stricter monitoring and regulation of sulfonated dyes in food products.[9,10] Industrial wastewater containing synthetic dyes, particularly from textiles and food-processing industries, presents a major environmental challenge. Aromatic sulfonates are characterized by high acidity ($pK_a < -1$), strong hydrophili-

*School of Consciousness, Dr. Vishwanath Karad MIT World Peace University, Kothrud 411038, Pune, India. E-mail: sudhirkumar.shinde@mitwpu.edu.in, rupali.patil@mitwpu.edu.in*

† These authors contributed equally.

city, and low *n*-octanol–water partition coefficients (log K > 2.2). As a result, these compounds exhibit high mobility in the aquatic system, and pass through wastewater treatment processes.[11]

Although conventional wastewater treatment methods include adsorption, flocculation, coagulation, ultrafiltration, reverse osmosis, and oxidation processes, these are inappropriate for industrial applications because of the high sludge generation and cost.[12] Consequently, it is difficult for current physical, chemical, and biological methods to effectively remove the color from dye-containing effluents, highlighting the need for efficient, cost-effective, and sustainable treatment technologies. The accurate detection and removal of dyes from foods and beverages remain a critical area of research. Several physicochemical quantification methods are limited due to high cost, low efficiency, high energy consumption, and secondary pollution.[13,14]

Common analytical techniques for dye detection include UV–Vis spectrophotometry and chromatographic techniques, such as thin layer chromatography (TLC), high-performance liquid chromatography (HPLC), capillary electrophoresis, liquid chromatography mass spectroscopy (LC-MS), and gas chromatography mass spectroscopy (GC-MS).[15] Although highly sensitive, these methods require efficient sample pre-treatment due to matrix interferences from soft drink components such as sugars, preservatives, and organic acids. Conventional pre-treatment strategies such as liquid–liquid extraction (LLE), solid-phase extraction (SPE), membrane extraction, and ion-exchange chromatography face challenges such as poor selectivity, high solvent usage, and limited reusability.[16] Sample treatment constitutes a critical phase that demands meticulous refinement to mitigate matrix interference and ensure compatibility with the specific food matrix under analysis. Therefore, the development of straightforward, selective, and effective pre-concentration and extraction methodologies is of paramount significance, particularly when coupled with the application of highly sensitive chromatographic and spectrometric techniques for the precise quantification of target dyes within diverse food matrices.

Molecularly imprinted polymer (MIP) technology offers a promising approach to address these problems. MIPs are synthetic polymers engineered with tailor-made recognition sites complementary in size, shape, and functional groups to a target molecule.[17–19] MIPs are prepared by polymerizing functional monomers and cross-linkers in the presence of a template molecule (*e.g.*, dye). Upon removal of the template, cavities with specific binding affinity to the dye remain. Compared to biological receptors such as antibodies, MIPs have gained popularity due to their robustness, thermal and chemical stability, low cost, and reusability. MIPs have proven effective in capturing various targets, ranging from small molecules to larger entities such as pharmaceuticals and pesticides,[20,21] peptides, proteins,[22] glycans,[23] and cells.[24,25] Nevertheless, further research is required to explore the synthesis and application of MIPs, especially for sulfonated food dyes or sulfated biomolecules.[26–29]

In recent years, there has been considerable research on sulfonated dye-selective MIPs, as evidenced by numerous studies (Table S1). These polymers are synthesized using a broad range of sulfonated dye templates, including Acid Black 1, Acid Black 210, Acid Brown 703, Acid Green 16, SY, Acid Violet 19, Cibacorn Red Dye, Direct Red 23, TZ, and Congo Red (CR). Researchers have investigated a variety of neutral and cationically charged functional monomers, such as acryloyloxyethyl trimethyl ammonium chloride, methacrylic acid, 1-(α-methyl acrylate)-3-methylimidazolium bromide, acrylamide, 1-vinyl imidazole, 3-aminopropyltrimethoxysilane, and titanium isopropoxide. These functional monomers play a key role in the interactions between the sulfonated groups of dye templates in the pre-polymerization stage and in stabilizing the monomer-template complex throughout polymerization, which ultimately shapes the binding sites within the MIP structure. Polar solvents, or their mixtures, are often preferred, particularly when sulfonated dyes act as templates, as this promotes stable pre-polymerization complexes – a pre-requisite for generating well-defined and effective recognition sites.

The effectiveness of MIPs is typically evaluated by comparing their performance against non-imprinted polymers (NIPs). Studies (Table S1) consistently show that MIPs exhibit higher dye-binding capacities and selectivity than NIPs. Because of this enhanced functionality, they are particularly well-suited for various applications, especially the removal of dyes from contaminated water sources. Dye-specific MIPs have been successfully used to bind and remove imprinted dyes from wastewater, river water, and industrial discharge. Despite these advantages, sulfonated dyes present several limitations when used as templates for synthesizing MIPs, including the introduction of additional environmental burden. The removal of the template from the polymer generates non-environmentally friendly solvent waste.

Another common technical issue arises from the use of protic polar solvents, which, while required to dissolve sulfonated dyes, can detrimentally impact monomer-template complexation when employed as a porogen. Specific sulfonated dye-imprinted materials, while effective for targeted dyes, often lack versatility due to their limited selectivity.

To address these challenges, we introduce herein a novel approach by creating class-selective MIPs designed for the general recognition of dyes containing phenyl sulfonate moieties. Phenyl sulfonic acid (PSA) is employed as a substructure template due to its non-toxic nature, cost-effectiveness, and prevalence of its structure in commercial sulfonated dyes.

We systematically explored the influence of polymer compositions and azo initiators on the molecular recognition, binding affinity, and binding capacity of templates, focusing on sulfonated dyes containing the PSA moiety. A comprehensive examination of the MIPs' recognition capabilities was conducted in pure water and polar environments containing potential interfering compounds, providing a thorough assessment of their selectivity and robustness. The applicability of the developed MIPs was demonstrated through successful recognition and extraction of target sulfonated dyes from

water, food samples, and soft drink samples, showcasing their potential for practical, real-world applications.

## Experimental

### Materials

Tetrabutylammonium hydroxide (TBAOH; 10% in methanol) and 95% ammonium hexafluorophosphate ($NH_4PF_6$) were received from Sisco Research Laboratory (SRL), India. Phenylsulfonic acid (PSA) was purchased from Avra Synthesis Private Limited, India. Ethylene glycol dimethacrylate (EGDMA) and 2-hydroxyethyl methacrylate (HEMA) were received from Otto Chemie Private Ltd, India. 1-Vinylimidazole (>98%) was received from TCI Japan. *N*,*N*′-Azo-bis(2,4-dimethyl)valeronitrile (ABDV) was received from Simson Pharma Limited, India. Dry MeCN was received from Merck USA. Sodium benzyl orange (Na-BO) was received from TCI, Japan. 2% TZ was received from Garden Flavours Company Private Ltd. 6% SY was received from Bakers Ville India Private Ltd; Alizarin Red S (AR), Metanil Yellow (MY), Fast Green FCF (FG), AM, and indigo carmine (IC) were received from Otto Chemie Private Ltd, India. Methyl orange (MO) and methylene blue (MB) were received from TCI, Japan.

37% hydrochloric acid (HCl) was received from Merck Life Sciences, India. HPLC grade 99.8% trifluoroacetic (TFA), HPLC grade methanol, HPLC grade MeCN, sodium chloride (NaCl), and 25% $NH_3$ solution were received from Loba Chemie Private Ltd, India. Glacial acetic acid was received from Clairo Filt India. The functional monomer 1-vinyl-3-{3-[(1-vinyl-1*H*-imidazol-3-ium-3-yl)methyl]benzyl}-1*H*-imidazol-3-ium bishexafluorophosphate (FM, $\mathbf{1^{2+}{\cdot}2PF_6^-}$) was synthesized according to a previously reported procedure.[29] EGDMA and HEMA were passed through a column of activated basic alumina to remove inhibitors, and were stored at −20 °C before polymerization.

### Synthesis of imprinted polymers (P1, P2, $P_N1$, $P_N2$)

The imprinted polymer P1 was prepared by dissolving the template TBA PSA (0.2 mmol; 79.7 mg) and the functional monomer $\mathbf{1^{2+}{\cdot}2PF_6^-}$ (0.2 mmol; 116.5 mg) complex in 1120 μL of dry MeCN. EGDMA (755 μL; 4 mmol) was added as a crosslinker to this monomer-template complex solution. For the imprinted polymer P2, a complex was formed by dissolving the template TBA PSA (0.4 mmol; 159.5 mg) and the functional monomer $\mathbf{1^{2+}{\cdot}2PF_6^-}$ (0.4 mmol; 227.5 mg) in 2240 μL of dry MeCN. The co-monomer HEMA (1.6 mmol; 195 μL) and EGDMA crosslinker (455 μL; 2.4 mmol) were added to the functional monomer template complex solution. For each polymer, 10 mg of the ABDV initiator was added to the above 10 mL screw-capped sintered vials containing the pre-polymerization solution. The solution was purged with a flow of dry nitrogen at room temperature for 5 min. The vials were closed with a lid and then sealed with silicone tape. Then, polymerization was carried out at 48 °C for 24 h in a preheated oven.

After polymerization, the glass vials were broken, and the bulk polymers were crushed into coarse particles. The template was removed from the polymers by shaking overnight in 1 N HCl, and again washed for 2 h in 1 N HCl, then 1 h in the 50 mL methanol: acetic acid: water/85 : 15 : 5 (v/v) solvent mixture, followed by two times with 50 mL of distilled water and a final wash with 50 mL of HPLC-grade methanol. The polymer was then dried in the oven at 40 °C for 2 h and thereafter subjected to fine grinding with a mortar and pestle to achieve particle sizes of 10–500 μm. The obtained particles, without sieving, were used to assess the binding properties. Reference polymers named NIPs $P_N1$ and $P_N2$, which contained different proportions of imprinted polymers, were prepared as described above, but in the absence of the template molecule from the pre-polymerization solution.

## Results and discussion

In a prior investigation, a unique tweezer-type dipodal functional monomer (FM) featuring imidazolium groups at the 1,3-positions of benzene rings and terminal vinyl polymerizable groups (illustrated in Fig. 1, $\mathbf{1^{2+}{\cdot}2PF_6^-}$) demonstrated significant interactions with sulfonates in acetonitrile. Thorave *et al.* reported the association constants ($K_a$) of the $\mathbf{1^{2+}{\cdot}2PF_6^-}$ : TBA PSA (FM : T) complex to be $6.17 \times 10^3$ $M^{-1}$ and $3.7 \times 10^3$ $M^{-1}$, as determined by UV and $^1H$ NMR titration at room temperature, respectively.[29] In our previous report, the stoichiometric complex, comprising TBA PSA and $\mathbf{1^{2+}{\cdot}2PF_6^-}$, was utilized in the production of MIPs using an EGDMA crosslinker, with and without the incorporation of a HEMA comonomer.[29] These polymers were synthesized *via* thermal polymerization in MeCN solvent using AIBN initiator at 65 °C.

Based on our previous findings, incorporating the hydrophilic HEMA comonomer into MIPs improves their water compatibility and enhances their ability to bind larger analytes containing phenyl sulfonate substructures. Azobisisobutyronitrile (AIBN) and ABDV are thermal azo initiators commonly used in free radical polymerization in organic solvents. ABDV is better suited for lower-temperature polymerization due to its lower decomposition temperature; its 10-hour half-life temperature is 51 °C, compared to 65 °C for AIBN. The polymerization temperature is expected to substantially influence the polymer's affinity and specificity,

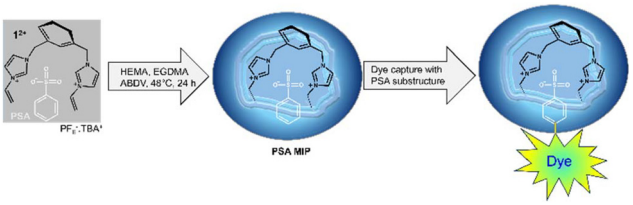


Fig. 1 Depiction of PSA recognition cavity in imprinted receptor and principle of capture dye containing PSA substructure. PSA MIP made from a complex of tweezer-type imidazolium functional monomers ($\mathbf{1^{2+}{\cdot}2PF_6^-}$ : FM) and TBA PSA template in the presence of HEMA comonomer (CM), EGDMA crosslinker (CL), and ABDV initiator at 48 °C.

thereby affecting the monomer-template complex and the polymerization process. Building on these prior results, the present study explored the polymerization of the $\mathbf{1}^{2+}\cdot\mathbf{2PF_6}^-$ : TBA PSA complex combined with the EGDMA crosslinker, either with or without the HEMA comonomer, using the azo initiator ABDV at 48 °C for 24 h in a conventional oven.

Inspired by the growing field of metal–organic framework (MOF)-derived porous functional polymers[30] and considering that bis-imidazolium functional monomers provide additional crosslinking density, the polymer composition was optimized by reducing the crosslinker concentration and increasing the monomer-template complex concentration, as detailed in Table 1. PSA-imprinted polymers (P1, P2) and reference polymers synthesized without TBA PSA and designated as non-imprinted polymers ($P_N1$, $P_N2$), were produced. The resulting polymers were processed into particulate form through manual grinding with a mortar and pestle, followed by extensive washing with 1 N HCl, acidic methanol, water, and methanol to eliminate any residual unreacted monomers and templates.

Optical microscopy and IR spectroscopy (Fig. S1) were employed to confirm polymer identity and ensure comparable morphology and composition. Subsequently, rebinding assays were conducted to assess the polymers' recognition abilities toward TBA PSA. Polymers were incubated in MeCN containing varying concentrations of TBA PSA (ranging from 0 to 5 mM), and the levels of unbound analyte in the supernatant were quantified using HPLC-UV (Fig. S2).

The amount of TBA PSA bound to the polymers was then calculated using eqn (S1). A Langmuir monosite binding model was applied to the data presented in Fig. S2 (eqn (S2)), allowing estimation of binding constants ($K_a$) and capacity ($B_{max}$). The fitting data, shown in Fig. S2 and summarized in Table 2, revealed an affinity ($K_a$) of P1 for the class 1 binding sites of $12.77 \times 10^3$ $M^{-1}$, which is 1.61 times greater than that of $P_N1$ ($K_a = 7.93 \times 10^3$ $M^{-1}$). The binding capacities ($B_{max}$) of P1 and $P_N1$ were determined as 99.69 ± 20.14 μmol $g^{-1}$ and 77.37 ± 12.95 μmol $g^{-1}$, respectively.

As depicted in Fig. 1, the imprinted polymer P1, featuring its PSA-specific cavities, exhibited superior affinity for TBA PSA, whereas the non-imprinted polymer $P_N1$ displayed lower affinity, confirming the successful imprinting of PSA within the imprinted polymers. The enhanced affinity of P1 underscores the effectiveness of the imprinting process in creating selective binding sites for the target analyte. In this study, we evaluated the imprinting capabilities of the P1/$P_N1$ (Fig. S2) and RP1/$RP_N1$ polymers (Fig. S3), which were synthesized using azo initiators at the polymerization temperatures for ABDV and AIBN[29] at 48 °C and 65 °C, respectively.

Our findings indicate that the RP1/$RP_N1$ polymer, synthesized with AIBN, exhibited a slightly lower imprinting effect ($K_a$ – $9.36 \times 10^3$ $M^{-1}$) compared to the P1/$P_N1$ polymers (Table 2). This observation is in alignment with the principle that the interaction strength between the imidazolium cation of the functional monomer and sulfonate-based anions, primarily facilitated by hydrogen bonding, exhibits an inverse relationship with temperature.[31] These results are consistent with previous studies indicating that reduced polymerization temperatures promote the formation of monomer-template complexes and the synthesis of MIPs through hydrogen bonding and electrostatic interactions, thereby influencing the characteristics and number of MIP recognition sites.[32,33] The rebinding isotherm data, analyzed using a one-site binding model for TBA PSA (Fig. S2 and Table 2), revealed a binding affinity (*K*a) of $23.81 \times 10^3$ $M^{-1}$ for P2. This value represents a 1.51-fold increase compared to the $K_a$ observed for $P_N2$ ($15.72 \times 10^3$ $M^{-1}$).

Interestingly, the binding capacity ($B_{max}$) for the NIPs $P_N1$ and $P_N2$ remained consistent at approximately 78 ± 11.2 μmol $g^{-1}$, indicating comparable saturation levels of bound analyte. However, a notable enhancement in binding capacity was observed for P2 (118 ± 18.15 μmol $g^{-1}$) when compared to P1. These findings suggest that polymers P2 and $P_N2$, characterized by a higher concentration of the monomer-template complex, exhibit superior binding characteristics, leading to improved affinity and capacity for the TBA PSA.

Polymer compositions of P2/$P_N2$ incorporating the template-functional monomer (T : FM) complex were synthesized

**Table 2** The binding constants ($K_a$) and specific binding capacities ($B_{max}$) for polymers P1, $P_N1$, P2, and $P_N2$ from the rebinding isotherm were obtained using TBA PSA in 100% MeCN and PSA and TZ in 100% $H_2O$

| Polymer : analyte | Rebinding solvent | $K_a$ ($\times 10^3$ $M^{-1}$) | $B_{max}$ (μmol $g^{-1}$) | Ref. Fig. (SI) |
|---|---|---|---|---|
| P1 : TBA PSA | 100% MeCN | 12.77 | 99.69 ± 20.14 | Fig. S2 |
| $P_N1$ : TBA PSA | | 7.93 | 77.37 ± 12.9 | |
| P2 : TBA PSA | | 23.81 | 118.1 ± 18.15 | |
| $P_N2$ : TBA PSA | | 15.72 | 78.08 ± 11.16 | |
| P1 : PSA | 100% $H_2O$ | 21.21 | 247.1 ± 18.1 | Fig. S4 |
| $P_N1$ : PSA | | 23.36 | 168.1 ± 7.45 | |
| P2 : PSA | | 15.89 | 309.4 ± 31.05 | |
| $P_N2$ : PSA | | 20.70 | 175.1 ± 9.6 | |
| P2 : TZ | 100% $H_2O$ | 24.27 | 129.2 ± 22.8 | Fig. 3 |
| PN2 : TZ | | 21.94 | 66.56 ± 15.98 | |

**Table 1** Polymer composition of PSA-imprinted polymers prepared by azo-initiated thermal polymerization in dry acetonitrile

| Polymer | Template (T, mmol) | Functional monomer (FM, mmol) | Comonomer (CM, mmol) | Crosslinker (CL, mmol) | Porogen (mL) |
|---|---|---|---|---|---|
| P1 | TBA PSA (0.2) | $\mathbf{1}^{2+}\cdot\mathbf{2PF_6}^-$ (0.2) | — | EGDMA (4) | MeCN (1.12 mL) |
| $P_N1$ | | $\mathbf{1}^{2+}\cdot\mathbf{2PF_6}^-$ (0.2) | — | EGDMA (4) | MeCN (1.12 mL) |
| P2 | TBA PSA (0.4) | $\mathbf{1}^{2+}\cdot\mathbf{2PF_6}^-$ (0.4) | HEMA (1.6) | EGDMA (2.4) | MeCN (2.24 mL) |
| $P_N2$ | | $\mathbf{1}^{2+}\cdot\mathbf{2PF_6}^-$ (0.4) | HEMA (1.6) | EGDMA (2.4) | MeCN (2.24 mL) |

with a T : FM : CM : CL ratio of 2 : 2 : 12 : 8 (in mmol). This represents a doubling of the T : FM ratio compared to previous polymers with a T : FM : CM : CL ratio of 1 : 1 : 12 : 8 (in mmol).[29] The T : FM ratio was also significantly higher than that of polymer P1/$P_N$1, which has a FM : T : CL ratio of 1 : 1 : 20 (in mmol), as shown in Table 1. The enhanced binding capacity in P2 (Table 2) suggests a higher concentration of monomer-template complex that can potentially generate a greater number of recognition sites.

Following the successful imprinting of TBA PSA in MeCN, polymer recognition of the PSA analyte in 100% water was assessed. As summarized in Table 2 and Fig. S4, all polymers demonstrated a binding affinity of roughly $2 \times 10^4$ $M^{-1}$. Polymer P2 exhibited a higher binding capacity for PSA ($B_{max}$ – 309.4 ± 31.05 μmol $g^{-1}$) as compared to P1 ($B_{max}$ – 247.1 ± 18.1 μmol $g^{-1}$).

The water-soluble synthetic azo dye, SY, which contains phenyl sulfonate moieties, was examined for its interaction with the P2 and $P_N$2 polymer particles. Briefly, 5 mg of each polymer was incubated in 4 ml of water containing 0.1 mM of the SY dye for 15 min. After removing the supernatant and washing with acidic and basic solvents, optical and fluorescence images were obtained using a red excitation filter and an exposure time of 700 ms. Fig. S5 displays fluorescence images revealing a significant difference in fluorescence intensity between the P2 and $P_N$2 particles. The P2 particles exhibited strong fluorescence, suggesting substantial SY retention. Conversely, $P_N$2 particles exhibited weak fluorescence, indicating a lower affinity for SY as compared to the imprinted polymer P2. The washing fractions were collected, and the combined fractions were quantified using HPLC-UV spectroscopy. The results were consistent with the fluorescence measurements, confirming that the imprinted polymer P2 retained ≥65% of the SY, whereas the non-imprinted polymer $P_N$2 retained only approximately 33%.

Based on preliminary data indicating improved selectivity of the produced imprinted polymer for SY dye, a quantitative examination of binding affinity and capacity was performed using TZ dye in an aqueous medium. TZ dye was selected as a suitable analyte for the rebinding experiments due to its structural features, particularly the presence of two phenyl sulfonate moieties, which were expected to favorably interact with the binding sites in the imprinted polymer matrix.

In the rebinding experiments, polymers P2 and $P_N$2 were accurately weighed (2.5 mg each) and suspended in 1 mL of TZ dye solution. A range of TZ dye concentrations spanning from 0 to 2 mM was prepared to generate a comprehensive rebinding isotherm. The suspensions were gently agitated on a shaker at room temperature for a duration of 100 min to ensure equilibrium. Following the incubation period, the samples were centrifuged at 10 000 rpm for 5 min to separate the polymer particles from the supernatant. The supernatant was carefully collected, analyzed using a multiplate reader, and the dye was compared to $P_N$2 and the reference sample.

To quantify the amount of TZ dye bound to the polymers, a rebinding isotherm was constructed (Fig. 3a). The isotherm was plotted with bound TZ (μmol $g^{-1}$) *versus* free TZ concentration, which fit with a one-site binding model (eqn (S2)). The concentration of TZ dye remaining in the supernatant was determined by measuring the absorbance at 430 nm using an external calibration curve. The UV-Vis spectra recorded at TZ concentrations of 0.2 mM (Fig. 3b) and 0.4 mM (Fig. 3c) showed that the polymer P2 has a markedly higher uptake of TZ dye compared to $P_N$2 and the reference sample. The rebinding analysis revealed similar affinity constants ($K_a$) of approximately $2 \times 10^4$ $M^{-1}$ for P2 and $P_N$2. However, the binding capacity of P2 (129.2 ± 22.8 μmol $g^{-1}$) was roughly twice that of $P_N$2 (Table 2), suggesting that the imprinting process significantly enhanced the TZ binding capacity of P2.

The sulfonated dyes shown in Fig. 2 include TZ (**1**), SY (**2**), FG (**3**), AM (**4**), AR (**5**), BO (**6**), IC (**7**), MY (**8**), and MO (**9**), all of which contain one, two, or three phenyl sulfonate moieties. These dyes were subjected to single-point rebinding assays, a design chosen to demonstrate the broad utility of MIPs for capturing sulfonated dyes bearing the template substructure. Methylene blue (MB, **10**), which lacks a phenyl sulfonate substructure, was included as a control. P2/$P_N$2 polymers (5 mg) were dispersed in 4 mL of aqueous solution containing individual dyes at concentrations of 1 mM for TZ, AR, and MY and 0.1 mM for SY, FG, AM, BO, IC, and MO.

After a 15 min settling period, 300 μL of the supernatant was analyzed using a multiplate reader (BioTek Synergy H) over a wavelength range of 230 to 900 nm. The absorbance spectra (Fig. 4a–i) showed that the P2 polymers exhibited higher dye uptake compared to the $P_N$2 polymers and the reference dye solution, as evidenced by the lower intensity of the P2 supernatant and visually confirmed by images of the

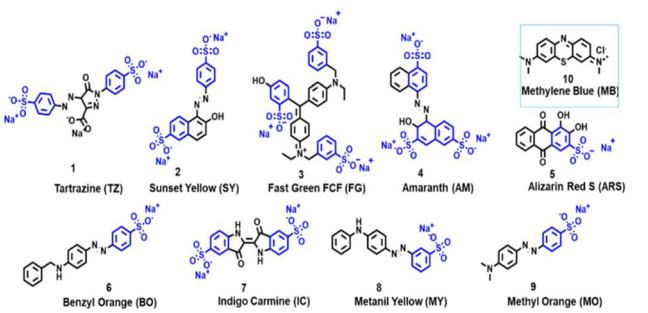


**Fig. 2** Chemical structure of sulfonated dyes (**1–9**) containing the PSA moiety and control dye (**10**) without the sulfonate group, used for the evaluation of P2 and $P_N$2 polymers.

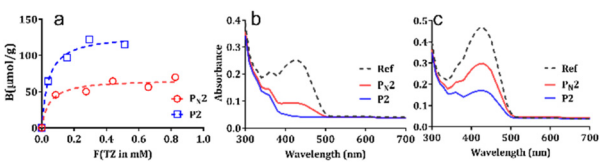


**Fig. 3** (a) Rebinding isotherm of TZ dye with P2 and $P_N$2 polymers in 100% water. Absorbance spectra of the supernatant after rebinding of TZ dye (1 mL) with 2.5 mg of polymer at concentrations of (b) 0.2 mM and (c) 0.4 mM TZ in 100% water.

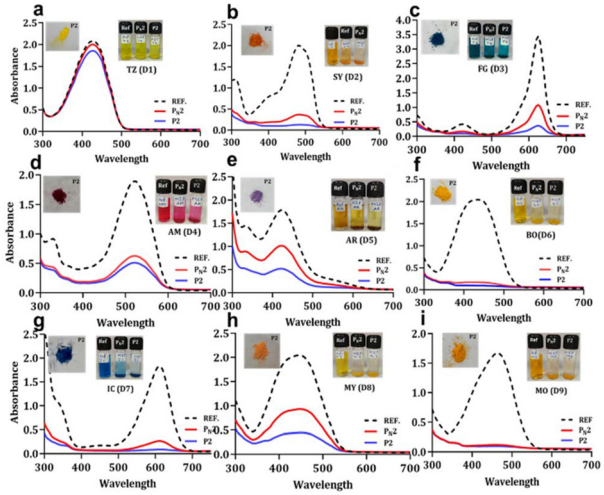


**Fig. 4** Binding of sulfonated dyes by P2 and $P_N2$ in 100% water. Absorption spectra of (a) TZ, (b) SY, (c) FG, (d) AM, (e) AR, (f) BO, (g) IC, (h) MY, and (i) MO, after incubation with P2 and $P_N2$, along with the reference spectrum for each dye solution. Inset: photographs of the dye-binding experiment in glass vials after 20 min, showing P2 polymers with captured dyes.

dye-bound P2 polymer (inset of Fig. 4a–i). In contrast, no significant differences were observed between P2, $P_N2$, and the reference MB dye solution (Fig. S6), with no visible changes in the supernatant solutions or dye-bound polymers.

Polymer P2 and $P_N2$ were subsequently evaluated for their direct interaction with sulfonated dyes in a selection of commercially available beverages. This set was composed of five distinct commercial drinks (Fig. S7): three carbonated beverages (CD1, CD2, CD3) and two fruit juices (CD4, CD5). The tested beverages contained a mixture of sugars and additives, including artificial sweeteners, flavorings, and preservatives, alongside the target sulfonated dyes. Notably, CD1 and CD3 contained caffeine at concentrations of 29 and 13 mg per 100 mL, respectively. The fruit juices CD4 and CD5 consisted of 10.5% orange juice from pulp and 5.1% mango pulp concentrate, respectively. The specific sulfonated dyes present were: Allura Red CD1, SY CD2, TZ CD3, a combination of TZ and SY CD4, and SY CD5.

Briefly, P2/$P_N2$ polymers (11 mg CD1, 5 mg CD2, 1 mg CD3, and 2.5 mg CD4 and CD5) were suspended in 4 mL of each soft drink, incubated for 15 min, and analyzed by UV-Vis spectroscopy (230–900 nm). These spectra were compared with those of $P_N2$ and the original soft drinks. The UV spectra (Fig. 5a, b, c, d, and Fig. S8) revealed that the polymer P2 adsorbed dyes from soft drinks to a greater extent than $P_N2$ and the reference drinks. Obvious visual differences among P2, $P_N2$, and soft drinks were also captured in the inset photographs of Fig. 5. These results indicate that MIPs can selectively recognize sulfonated dyes in complex soft drink matrices, where high polarity and interference from sugar, organic acids, and preservatives are present.

MY is an unapproved food colorant from the yellow azo dye class and is used worldwide,[34] finding diverse applications in

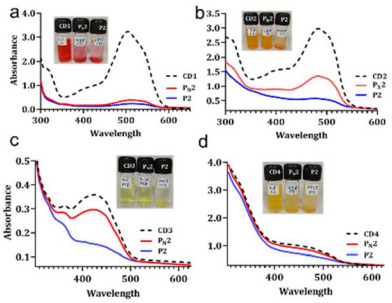


**Fig. 5** Sulfonate dye binding by P2 and $P_N2$ in soft drink CD1–CD4. Absorption spectra of (a) CD1, (b) CD2, (c) CD3, and (d) CD4 after polymer treatment; reference spectra of the original soft drinks. Inset: photographs of the dye binding experiment in glass vials after 25 min.

the wool, silk, paper ink, and aluminium industries. Despite its industrial versatility, MY consumption poses significant health risks. Studies have linked MY exposure to neurotoxicity, carcinogenicity, and genotoxicity, with harmful effects on critical organs such as the brain, liver, kidneys, testes, and ovaries.[35] Concerns have been raised about its presence in food products, particularly turmeric, especially those processed by unorganized sectors.

To investigate the presence of MY, four samples of non-food grade turmeric powder were obtained from local markets. Sample preparation involved dissolving 200 mg of turmeric powder into 10 mL of water. Following this, 1 mL of the supernatant solution was used for MY dye extraction using 2 mg of P2/$P_N2$ polymer. After washing with acidic and basic solvents, two elution fractions were dried by evaporation and reconstituted in water. The extracted MY dye was analyzed by the C18-HPLC-UV method. Analysis of HPLC spectra from eluted fractions (Fig. 6), coupled with the quantified MY dye data (Table S2), demonstrated that the P2 polymer displayed a superior binding affinity for MY dyes extracted from the collected samples, as compared to $P_N2$. MY was detected in three of four turmeric samples at concentrations ranging from 0.7 to

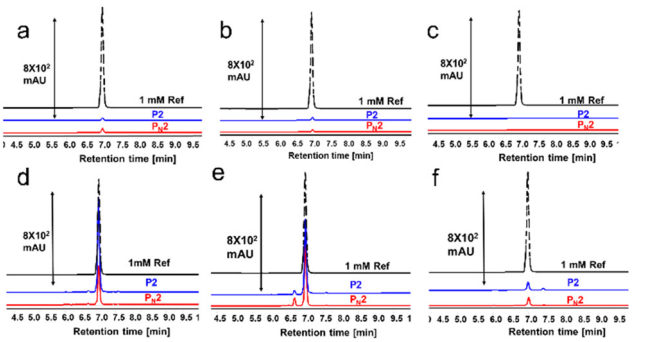


**Fig. 6** C18-HPLC-UV spectra of eluted fractions of P2 and $P_N2$ after MY dye extraction from three turmeric samples. Elution fraction 1: (a) sample 1 (b) sample 2, and (c) sample 3 and elution fraction 2: (d) sample 1, (e), sample 2, and (f) sample 3. In each panel, the spectra from P2 and $P_N2$ are overlaid for direct comparison.

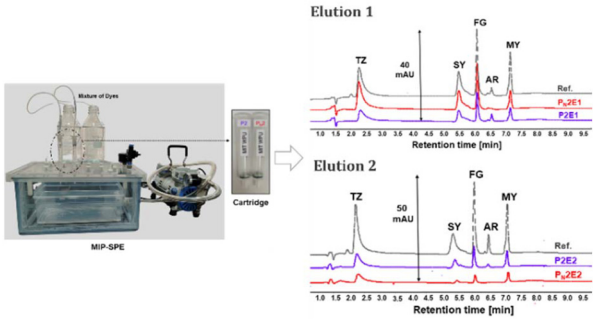


**Fig. 7** (a) MIP-SPE units with P2 and $P_N2$ cartridges. (b) C18-HPLC-UV chromatograms of eluted fractions (E1, E2) from P2 and $P_N2$ cartridges after extraction of a dye mixture (TZ, SY, FG, AR, and MY; $4.5 \times 10^{-8}$ M) in 1 L water. Ref: dye mixture in elution solvent. Peaks are labelled with dye names.

9 mg per gram of turmeric (Table S2). Sample 4 showed no detectable MY (Fig. S9).

As a proof-of-concept, the effectiveness of synthesized MIPs for dye extraction from water was evaluated using P2 and $P_N2$ as solid phase extraction (SPE) sorbents. For MIP-SPE, 20 mg of P2/$P_N2$ polymers was packed into 3 mL cartridges (Fig. 7). An equimolar mixture of TZ, MY, FG, AR, and SY dyes (each at 45 nM) was added to 1 L of water. The water, which contained a mixture of mono-, di-, and tri-sulfonated dyes, was passed through the P2/$P_N2$ cartridges at a flow rate of 2.5 mL $min^{-1}$ under a vacuum of approximately 30 mm Hg. After drying the polymer, adsorbed dyes were eluted in two steps (E1, E2) using acidic methanol. The eluted fractions were quantified *via* C18-HPLC-UV and compared with reference samples.

As shown in Fig. S10, the combined elution fractions for MIP and NIP exhibited similar abilities to adsorb water-soluble dyes, with a slight preference for multi-sulfonated over mono-sulfonated dyes, yielding recoveries ranging from 50% to 90% in water. Notably, chromatograms (Fig. 7) revealed higher dye concentrations in the E2 fractions from P2 compared to $P_N2$, in contrast to E1 fractions. This suggests that P2 polymers retain sulfonated dyes more strongly than the corresponding NIPs.

## Conclusions

In this study, we developed class-selective molecularly imprinted polymers (MIPs) for the recognition of sulfonated dyes using a substructure imprinting approach with phenyl sulfonic acid (PSA) as the template, and a tweezer-type bis-imidazolium functional monomer. The optimal conditions—lower polymerization temperature (48 °C) with ABDV initiator and a higher template-to-monomer ratio (P2 formulation)—markedly enhanced binding capacity and affinity. The MIPs created using HEMA and EGDMA with optimized compositions demonstrated increased water compatibility compared to MIPs synthesized without HEMA. Notably, the optimized polymer (P2) demonstrated a binding capacity of 300 μmol $g^{-1}$ and an affinity constant ($K_a$) of $1.6 \times 10^4$ $M^{-1}$ for PSA and for structurally diverse sulfonated dyes (including TZ, SY, FG, AM, AR, BO, IC, MY, and MO) in both organic and aqueous solvents. These MIPs successfully recognized and bound sulfonated dyes even in complex matrices such as commercial soft drinks containing carbohydrates, organic acids, preservatives, and caffeine.

Importantly, we demonstrated for the first time that imprinted polymers can be used to capture food dyes from adulterated turmeric samples, highlighting their potential application in food safety monitoring. As a proof-of-concept, developed MIPs were employed as adsorbents in solid phase extraction (SPE) cartridges, enabling the capture of a mixture of ultra-traces of sulfonated dyes from water.

Collectively, these findings establish that substructure-imprinted MIPs offer a promising, selective, and robust platform for the extraction and preconcentration of sulfonated dyes from complex food and environmental matrices, with significant implications for public health protection and environmental monitoring.

## Author contributions

This manuscript was written through the contributions of all authors. All authors approved the final version of the manuscript.

## Conflicts of interest

There are no conflicts to declare.

## Data availability

Supplementary information (SI): experimental details (materials, methods, HPLC), additional references (**10**) for imprinted polymers targeting sulfonated dyes (Table S1), IR (Fig. S1), optical and fluorescence microscopy images (Fig. S5), rebinding isotherms and fitting data (Fig. S2–S4), and additional supporting evidence such as UV and HPLC spectra (Fig. S6–S10). See DOI: https://doi.org/10.1039/d6lp00048g.

## Acknowledgements

We highly acknowledge the financial support from Prof. Dr. Vishwanath Karad for providing a starting research grant to the School of Consciousness, Dr. Vishwanath Karad MIT World Peace University, Kothrud Pune, India.

## References

1 R. Al-Tohamy, S. S. Ali, F. Li, K. M. Okasha, Y. A. G. Mahmoud, T. Elsamahy, H. Jiao, Y. Fu and J. Sun, *Ecotoxicol. Environ. Saf.*, 2022, **231**, 113160.

2 GVR (2023) onlinehttps://www.grandviewresearch.com/industry-analysis/food-colorants-market.
3 P. Barciela, A. Perez-Vazquez and M. A. Prieto, *Food Chem. Toxicol.*, 2023, **178**, 113935.
4 S. I. Kaya, A. Cetinkaya and S. A. Ozkan, *Food Chem. Toxicol.*, 2021, **156**, 112524.
5 O. I. Lipskikh, E. I. Korotkova, Y. P. Khristunova, J. Barek and B. Kratochvil, *Electrochim. Acta*, 2018, **260**, 974–985.
6 T. Li, L. Wei, Y. Fang, Y. Cui, X. Wang and Y. Li, *Environ. Pollut.*, 2025, **386**, 127180.
7 A. Lehmkuhler, M. D. Miller, A. Bradman, R. Castorina, M.-A. Chen, T. Xie and A. E. Mitchell, *J. Food Compos. Anal.*, 2022, **112**, 104649.
8 N. Martins, C. L. Roriz, P. Morales, L. Barros and I. C. F. R. Ferreira, *Trends Food Sci. Technol.*, 2016, **52**, 1–15.
9 P. Amchova, H. Kotolova and J. Ruda-Kucerova, *Regul. Toxicol. Pharmacol.*, 2015, **73**, 914–922.
10 E. K. Dunford, T. M. Galligan, L. S. Taillie and A. A. Musicus, *J. Acad. Nutr. Diet.*, 2025, **125**, 1207–1217.e9.
11 R. Loos and R. Niessner, *J. Chromatogr. A*, 1998, **822**, 291–303.
12 A. Ahmad, S. H. Mohd-Setapar, C. S. Chuong, A. Khatoon, W. A. Wani, R. Kumar and M. Rafatullah, *RSC Adv.*, 2015, **5**, 30801–30818.
13 Y. Shi, Z. Yang, L. Xing, X. Zhang, X. Li and D. Zhang, *World J. Microbiol. Biotechnol.*, 2021, **37**, 137.
14 S. Dutta, B. Gupta, S. K. Srivastava and A. K. Gupta, *Mater. Adv.*, 2021, **2**, 4497–4531.
15 K. Yamjala, M. S. Nainar and N. R. Ramisetti, *Food Chem.*, 2016, **192**, 813–824.
16 O. S. Salami, M. Sihlahla, B. S. Dladla and N. Mketo, *Trends Food Sci. Technol.*, 2025, **160**, 104991.
17 B. Sellergren, *TrAC, Trends Anal. Chem.*, 1997, **16**, 310–320.
18 B. Sellergren, *Molecularly imprinted polymers man-made mimics of antibodies and their applications in analytical chemistry*, Elsevier Amsterdam, 1st edn, 2000.
19 D. A. Gkika, A. K. Tolkou, D. A. Lambropoulou, D. N. Bikiaris, P. Kokkinos, I. K. Kalavrouziotis and G. Z. Kyzas, *RSC Appl. Polym.*, 2024, **2**, 127–148.
20 C. Alexander, H. S. Andersson, L. I. Andersson, R. J. Ansell, N. Kirsch, I. A. Nicholls, J. O'Mahony and M. J. Whitcombe, *J. Mol. Recognit.*, 2006, **19**, 106–180.
21 J. J. BelBruno, *Chem. Rev.*, 2019, **119**, 94–119.
22 B. Tse Sum Bui, A. Mier and K. Haupt, *Small*, 2023, **19**, 2206453.
23 P. Li and Z. Liu, *Chem. Soc. Rev.*, 2024, **53**, 1870–1891.
24 S. Piletsky, F. Canfarotta, A. Poma, A. M. Bossi and S. Piletsky, *Trends Biotechnol.*, 2020, **38**, 368–387.
25 F. Ding, Y. Ma, W. Fan, J. Xu and G. Pan, *Trends Biotechnol.*, 2024, **42**, 1097–1111.
26 S. Ambrosini, M. Serra, S. Shinde, B. Sellergren and E. De Lorenzi, *J. Chromatogr. A*, 2011, **1218**, 6961–6969.
27 S. Shinde, A. Bunschoten, J. A. W. Kruijtzer, R. M. J. Liskamp and B. Sellergren, *Angew. Chem., Int. Ed.*, 2012, **51**, 8326–8329.
28 S. Shinde, A. Incel, M. Mansour, G. D. Olsson, I. A. Nicholls, C. Esen, J. Urraca and B. Sellergren, *J. Am. Chem. Soc.*, 2020, **142**, 11404–11416.
29 R. Thorave, M. Celentano, K. Bankar, B. Sellergren, P. Manesiotis and S. A. Shinde, *Polym. Sci. Technol.*, 2025, **1**, 488–499.
30 S. K. Firooz and D. W. Armstrong, *Anal. Chim. Acta*, 2022, **1234**, 340208.
31 N. R. Pitawela and S. K. Shaw, *ACS Meas. Sci. Au*, 2021, **1**, 117–130.
32 Y. Lu, C. Li, X. Wang, P. Sun and X. Xing, *J. Chromatogr. B: Anal. Technol. Biomed. Life Sci.*, 2004, **804**, 53–59.
33 E. V. Piletska, A. R. Guerreiro, M. J. Whitcombe and S. A. Piletsky, *Macromolecules*, 2009, **42**, 4921–4928.
34 I. S. Khan, M. N. Ali, R. Hamid and S. A. Ganie, *Toxicol. Rep.*, 2020, **7**, 370–375.
35 T. N. Nagaraja and T. Desiraju, *Food Chem. Toxicol.*, 1993, **31**, 41–44.